International Journal of Hydrogen Energy 138 (2025) 1004–1016

Contents lists available at ScienceDirect

International Journal of Hydrogen Energy

journal homepage: www.elsevier.com/locate/he

A refined method of identifying NO_x formation by NH_3 and N_2 for ammonia combustion

Shuang Li [a], Jicang Si [a,*], Xiangtao Liu [b], Yuanye Guo [a], Guochang Wang [c], Enguang Xu [d], Jialin Zou [a], Qiuhao Zhang [a], Minyi Xu [a], Jianchun Mi [b,e]

[a] Marine Engineering College, Dalian Maritime University, Dalian, 116026, PR China
[b] College of Engineering, Peking University, Beijing, 100871, PR China
[c] State Key Laboratory of Clean and Efficient Coal Utilization, Taiyuan University of Technology, Taiyuan, 030024, PR China
[d] Dalian Shipbuilding Industry Co., Ltd., Dalian, 116026, PR China
[e] Ningbo Institute of Digital Twin, Ningbo, 315201, PR China

ARTICLE INFO

Handling Editor: Prof B Shabani

Keywords:
Ammonia combustion
Reaction mechanism
NO_x formation
Nitrogen source identification

ABSTRACT

This paper presents a refined method for explicitly identifying the contributions of NH_3 and N_2 to NO_x formation. The approach modifies the nitrogen element in N_2 to N*N*, effectively decoupling the reactions originating from both N_2 and NH_3 within the chemical reaction mechanism. Building on the previous work by Wu et al. (*Energy*, 2023, 284, 129291–129303), this study further refines the process of reaction differentiation, particularly under rotational asymmetric multi-nitrogen atom structures, enabling more accurate identification of reaction pathways for different nitrogen source. Notably, a rigorous method is introduced, along with a set of principles for distributing reaction kinetics parameters. This approach is applicable for distinguishing specific elements in both the fuel and oxidizer during the combustion process.

The proposed method is then applied to develop a new mechanism comprising 74 species and 946 reactions, based on the mechanism by Zhang et al. (*Combust. Flame*, 2021, 234, 111653–111667). The proposed method successfully uncouples the NO_x formation pathways, revealing intricate interactions between NH_3- and N_2-derived intermediates, and elucidating their roles in the formation of NO, NO_2, and N_2O under varying conditions of temperature, oxygen concentration, and equivalence ratio. Key findings include the temperature-dependent transition of dominant NO_x sources, cross-pathway interactions between NH_3 and N_2, and shifts in formation and reduction pathways. Notably, the present study demonstrates that interactions between NH_3-derived and N*N*-derived nitrogen species represent a primary NO consumption pathway at elevated combustion temperatures, particularly through reactions such as $N + N^*O \rightarrow N^*N + O$ and $N^* + NO \rightarrow N^*N + O$. Additionally, when the initial reactant temperature approaches approximately 800 K, an overall reduction in total NO formation is observed, despite the enhanced formation of thermal NO at these higher combustion temperatures.

1. Introduction

The development of human society is deeply intertwined with energy production, and combustion has long served as a primary energy source. However, the widespread reliance on fossil fuels has led to substantial environmental challenges, particularly global warming driven by carbon dioxide (CO_2) emissions. This has created an urgent need for sustainable, low-carbon energy alternatives. Ammonia (NH_3) has emerged as a promising carbon-free fuel that could significantly reduce greenhouse gas emissions. Despite its potential, practical applications of NH_3 are hindered by several challenges compared to conventional hydrocarbon fuels, ammonia exhibits poor combustion stability due to its low reactivity, narrow flammability limits, and low laminar flame speed [1,2], which can lead to issues such as flame extinction under traditional combustion modes [3,4]. To address these issues, researchers have explored various strategies, such as increasing combustion temperature [5], raising oxygen concentration [6], blending active fuels [7–9], pressurized combustion [10,11], plasma-assisted combustion [12].

* Corresponding author.
E-mail address: sjc@dlmu.edu.cn (J. Si).

https://doi.org/10.1016/j.ijhydene.2025.05.206
Received 24 February 2025; Received in revised form 6 May 2025; Accepted 14 May 2025

Table 1
Composition of nitrogen elements before and after source identification, considering the symmetry and asymmetry of the substances being distinguished.

Before differentiation	After differentiation	Before differentiation	After differentiation
N_2	N_2, N*N, N*N*	NO	NO, N*O
N	N, N*	N_2O	N_2O, N*NO,
NH	NH, N*H		NN*O, N*N*O
NH_2	NH_2, N*H_2	NO_2	NO_2, N*O_2
NH_3	NH_3, N*H_3	HNO	HN*O
N_2H_2	N_2H_2, N*HNH,	HON	HON*
	N*HN*H	HONO	HON*O
N_2H_3	N_2H_3, N*HNH_2,	H_2NO	H_2N*O
	NHN*H_2, N*HN*H_2	HNOH	HN*OH
H_2NN	H_2NN, H_2N*N,	NH_2OH	N*H_2OH
	H_2NN*, H_2N*N*	HNO_2	HN*O_2
N_2H_4	N_2H_4, N*H_2NH_2,	$HONO_2$	HON*O_2
	N*H_2N*H_2	NO_3	N*O_3
H_2NN	H_2NN, H_2N*N,	HNO_3	HN*O_3
	H_2NN*, H_2N*N*		

Nevertheless, a major barrier remains: high emissions of nitrogen oxides (NO_x) produced during NH_3 combustion [13]. Kinetic studies show that NO is the primary NO_x component at atmospheric pressure, formed via the pathway $NH_3 \rightarrow NH_2 \rightarrow HNO \rightarrow NO$, and the key reactions are [14–17]:

$$NH_2 + O \leftrightarrow HNO + H \quad (R1)$$

$$NH + OH \leftrightarrow HNO + H \quad (R2)$$

$$HNO + OH \leftrightarrow NO + H_2O \quad (R3)$$

with HNO acting as a crucial intermediate [18]. Okafor et al. [19] emphasize the importance of the reaction $NH_2 + O \leftrightarrow HNO + H$ in NO formation and flame propagation speed. Wang et al. [20] reported that the HNO pathway is the primary route for NO formation, accounting for more than 50% of total NO generation, while over 40% of NO consumption results from reactions involving NO and NH_i species. Under fuel-lean conditions, elevated concentrations of O and OH radicals enhance the NH_i pathway, increasing its significance in NO formation [21]. Liu et al. [22] demonstrated that under fuel-rich conditions, the decreased concentration of atomic oxygen suppresses NO formation through the NH_i pathway, causing H radicals to become significant in promoting NO formation via the HNO route. Zhang et al. [23] further observed that heat losses near wall regions inhibit the critical chain-branching reaction $H + O_2 \rightarrow OH + O$, resulting in localized reductions of OH concentrations, thus suppressing NO formation through both the HNO and NH pathways. In oxygen-rich environments, NO can be further oxidized to N_2O, particularly under lean combustion conditions. Hayakawa et al. [24] demonstrated that the equivalence ratio strongly influences NO_x emissions in NH_3 flames. Under fuel-lean conditions, elevated flame temperatures promote OH radical production, resulting in NO concentrations exceeding 1000 ppm. Conversely, fuel-rich conditions suppress NO_x formation via the DeNO$_x$ pathway but may lead to increased emissions of unburned NH_3. Tang et al. [25] investigated ammonia combustion in a jet-stirred reactor (JSR) and found that the equivalence ratio plays a crucial role in the formation of NO_2 and N_2O, particularly under extremely lean conditions. As the equivalence ratio increases, HO_2 concentrations decrease, suppressing reactions such as $NO + HO_2 \leftrightarrow NO_2 + OH$ and $NH_2 + NO_2 \leftrightarrow N_2O + H_2O$. Further studies by Okafor et al. [26,27] and Khateeb et al. [28] revealed that N_2O formation is influenced by wall heat loss and combustion residence time, making it a prominent byproduct in lean, low-temperature environments. These findings are further validated by Zhu et al. [29] in gas turbines. Combustion pressure is another factor that significantly affects NO_x formation. Elevated pressures promote reactions like $H + OH + M \leftrightarrow H_2O + M$, which reduce OH radical concentrations and suppress NO formation [27,30]. However, García-Ruiz et al. [31] found that higher pressures decrease NO emissions but simultaneously increase N_2O production due to changes in reaction kinetics, reflecting the complex interplay between pressure and NO_x formation pathways.

In pure ammonia combustion, NO_x emissions can be classified into two categories based on their nitrogen source: fuel-derived NO_x from NH_3 and oxidizer-derived NO_x from N_2 [32]. Understanding the nitrogen source of NO_x is critical for developing effective emission reduction strategies. Fuel-derived NO_x pathways, including the Extended Zeldovich, HNO, NH_i and NNH pathways, are predominant in ammonia combustion, particularly under stoichiometric and fuel-rich conditions. Among these, The HNO pathway, characterized by the reaction $HNO + O \rightarrow NO + OH$, is particularly sensitive to flame temperature and radical concentrations [33,34]. Similarly, the NH_i pathway (NH, NH_2, and NH_3 intermediates) drives NO formation through temperature-dependent reactions such as $NH + O \rightarrow NO + H$ and $NH_2 + O \rightarrow NO + H_2$ [34].

Table 2
Composition of nitrogen elements before and after source identification, considering the symmetry and asymmetry of the substances being distinguished (N_2O in case (ii)), the units for A, E_a are $(cm^3/mol)^{n-1}/s$ and cal/mol.

Case	Before source identification	A	b	E_a	After source identification	A	b	E_a
Case (i)	R45 $N + O_2 \leftrightarrow NO + O$	5.841E9	1.01	6202.0	$N + O_2 \leftrightarrow NO + O$	5.841E9	1.01	6202.0
					$N^* + O_2 \leftrightarrow N^*O + O$	5.841E9	1.01	6202.0
Case (ii)	R185 $NH_2 + NH \leftrightarrow NH_3 + N$	9574.0	2.46	107.3	$NH_2 + NH \leftrightarrow NH_3 + N$	9574.0	2.46	107.3
					$N^*H_2 + NH \leftrightarrow N^*H_3 + N$	9574.0	2.46	107.3
					$NH_2 + N^*H \leftrightarrow NH_3 + N^*$	9574.0	2.46	107.3
					$N^*H_2 + N^*H \leftrightarrow N^*H_3 + N^*$	9574.0	2.46	107.3
	R81 $NH + NO \leftrightarrow N_2O + H$	2.7E15	−0.78	20.0	$NH + NO \leftrightarrow N_2O + H$	2.7E15	−0.78	20.0
					$N^*H + NO \leftrightarrow N^*NO + H$	2.7E15	−0.78	20.0
					$NH + N^*O \leftrightarrow NN^*O + H$	2.7E15	−0.78	20.0
					$N^*H + N^*O \leftrightarrow N^*N^*O + H$	2.7E15	−0.78	20.0
Case (iii-1)	R173 $NH + NH \leftrightarrow NH_2 + N$	0.57	3.88	342.0	$NH + NH \leftrightarrow NH_2 + N$	0.57	3.88	342.0
					$N^*H + N^*H \leftrightarrow N^*H_2 + N^*$	0.57	3.88	342.0
					$N^*H + NH \leftrightarrow N^*H_2 + N$	0.57	3.88	342.0
					$N^*H + NH \leftrightarrow NH_2 + N^*$	0.57	3.88	342.0
					$N^*H + NH \rightarrow N^*H_2 + N$	0.57	3.88	342.0
					$N^*H + NH \rightarrow NH_2 + N^*$	0.57	3.88	342.0
Case (iii-2)	R271 $NH_2 + NH_2 \leftrightarrow N_2H_2 + H_2$	1.7E8	1.62	1.1783E4	$NH_2 + NH_2 \leftrightarrow N_2H_2 + H_2$	1.7E8	1.62	1.1783E4
					$N^*H_2 + N^*H_2 \leftrightarrow N^*HN^*H + H_2$	1.7E8	1.62	1.1783E4
					$N^*H_2 + NH_2 \leftrightarrow N^*HNH + H_2$	1.7E8	1.62	1.1783E4
					$N^*H_2 + NH_2 \rightarrow N^*HNH + H_2$	5.1E08	1.62	1.1783E4
Case (iv)	R774 $NO + O(+M) \leftrightarrow NO_2(+M)$	2.95E14	−0.4	0.0	$NO + O(+M) \leftrightarrow NO_2(+M)$	2.95E14	−0.4	0.0
					$N^*O + O(+M) \leftrightarrow N^*O_2(+M)$	2.95E14	−0.4	0.0

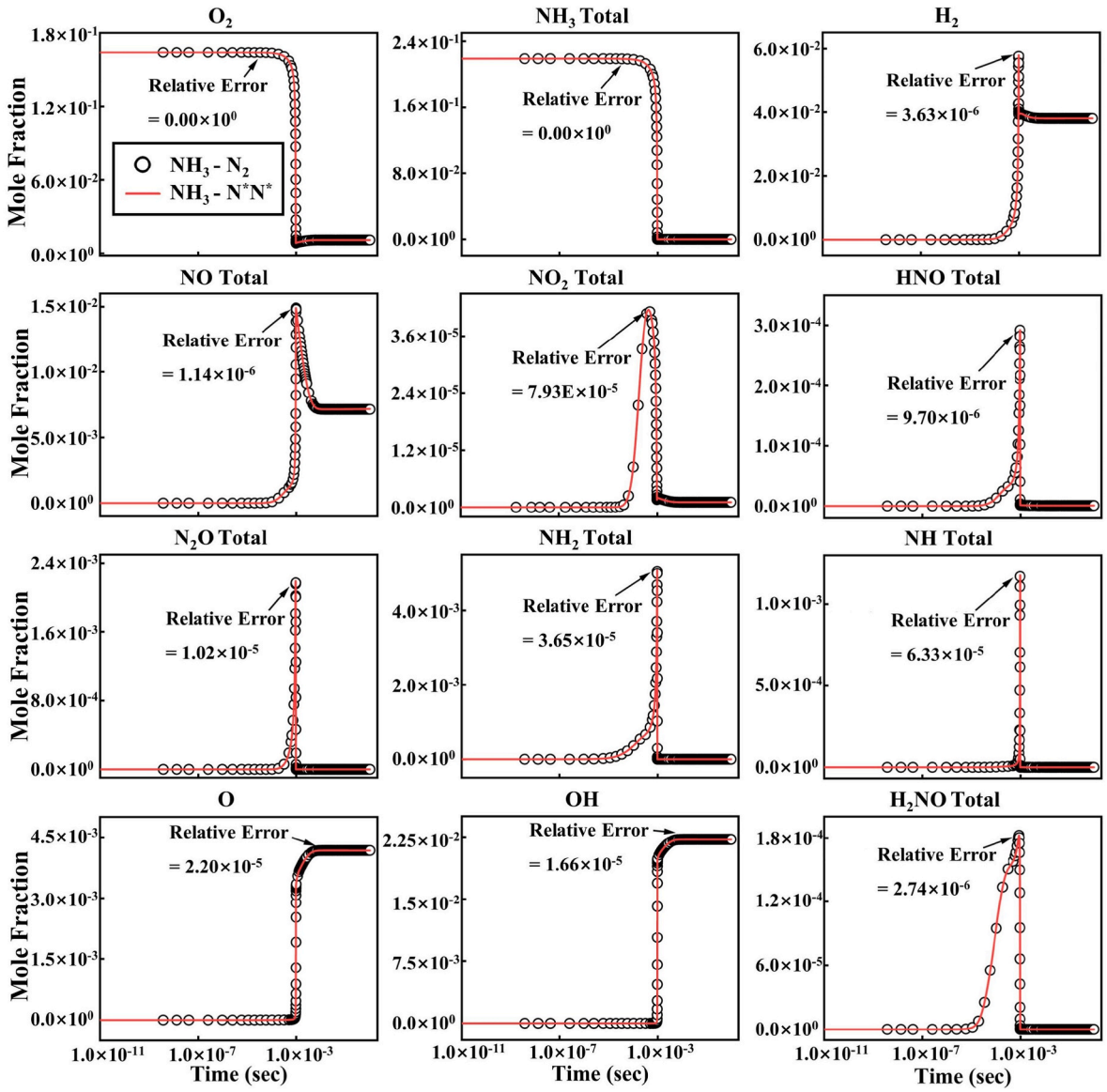

Fig. 1. Conversion processes of various species in PSR at $T_{initial} = 1600$ K, $X_{O2} = 0.21$, and $\Phi = 1$. Results are calculated by mechanism without nitrogen source identification ($NH_3/N_2/O_2$) and nitrogen source identification ($NH_3/N^*N^*/O_2$).

The NNH pathway, involving $NH_2 + NO \rightarrow NNH + OH$, further contributes to NO formation under specific conditions [35]. N_2-sourced NO_x pathways involve nitrogen from ambient air and include thermal, N_2O-intermediate, prompt NO_x, and NNH mechanisms [36], which are largely investigated previously for hydrocarbon fuel combustion.

To accurately distinguish NO_x formation originating from NH_3, Yan et al. [37] and Yang et al. [38] utilized inert argon (Ar) to replace atmospheric N_2, thereby isolating NH_3-derived NO_x formation pathways. Similarly, Zhao et al. [39] and Yang et al. [40] employed artificial non-reactive N_2 distinctly investigate NH_3-derived NO_x formation pathways. Li et al. [41] proposed an alternative method involving combustion of NH_3 and hydrogen (H_2) at identical flame temperatures, attributing observed discrepancies in NO_x formation solely to nitrogen oxidation in NH_3.

Recent work by Liu et al. [22] further emphasized the complexity of NO_x formation during pure NH_3 combustion, demonstrating the critical role of the Zeldovich mechanism in NO consumption. These findings indicate complex interactions between nitrogen species derived from both NH_3 and atmospheric N_2, which share common pathways but may exhibit opposing effects. Thus, differentiating NH_3-derived from N_2-derived NO_x pathways and elucidating their interactions are essential for understanding NO_x formation mechanisms in ammonia combustion.

Yan et al. [42] and Yang et al. [43–45] were the first to propose a method to distinguish nitrogen originating from ammonia (NH_3) and atmospheric nitrogen (N_2) within combustion simulations. Specifically, they introduced labeled nitrogen species (N^{**}_2 or N_{air2}) to replace atmospheric N_2, assigning thermal NO_x pathways to these labeled species, thereby decoupling the formation of fuel-derived and thermal NO_x formation during combustion. Despite this advancement, interactions between nitrogen species derived from NH_3 and N_2 remained unexplored.

To address this, Wu et al. [46] introduced a nitrogen-labeling approach, labeling atmospheric nitrogen as NN* and N^*_2, to clearly distinguish thermal NO_x from fuel-derived NO_x while explicitly incorporating their interactions. However, this method did not account for structural complexities associated with rotational asymmetry in multi-nitrogen atom species (e.g., distinguishing, N*NO vs. NN*O) and their implications for reaction product formation. For example, in the reverse reaction of $N_2O + H \leftrightarrow NH + NO$, cleavage of the N–N bond explicitly results in NO formation from the nitrogen atom bonded to

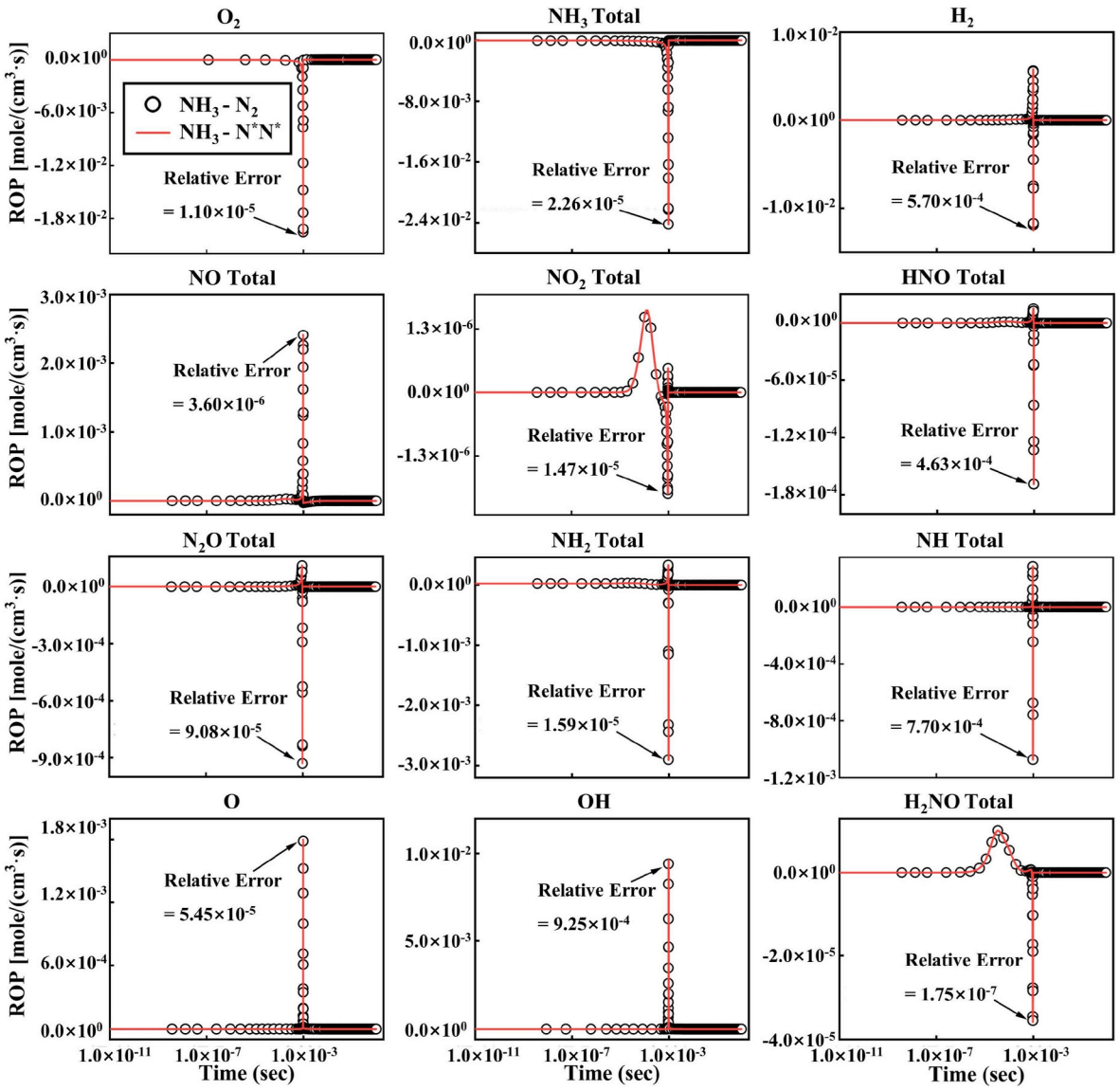

Fig. 2. Rate of production (ROP) for NH_3 combustion in PSR at $T_{initial} = 1600$ K, $X_{O2} = 0.21$, and $\Phi = 1$. Results are calculated by new mechanism without nitrogen source identification ($NH_3/N_2/O_2$) and with nitrogen source identification ($NH_3/N^*N^*/O_2$).

oxygen, whereas the nitrogen atom distant from oxygen combines with hydrogen, forming NH. Furthermore, previous approaches inadequately described the detailed mechanism construction, derivation of reaction kinetics parameters, and potential errors introduced by nitrogen labeling.

To further refine the differentiation of nitrogen transformations from both NH_3 and N_2 sources, the present study refines and systematically extends the method proposed by Wu et al. [46]. Specifically, the present work systematically details the construction of the nitrogen-labeling mechanism and provides a rigorous approach for assigning kinetic parameters. With this method, the present study also develop a new mechanism with 74 species and 946 reactions based on the detailed mechanism by Zhang et al. [47] The study discusses the contributions of different NO_x sources, the interactions between nitrogen species from NH_3 and N_2, and provides a comparison with the artificial species method.

2. Derivation of nitrogen element source identification method and construction of new mechanism

This study presents a refined method, building on the work of Wu et al. [46], to distinguish nitrogen-containing species derived from both NH_3 and N_2 in combustion simulation. The primary objective of this method is to differentiate the pathways leading to NO_x formation, while accounting for the multi-nitrogen species with rotational asymmetry structures. By identifying nitrogen elements based on their sources (e.g., NH_3 and N*N*, N* stands for the nitrogen source from N_2), the method allows for the identification of the corresponding reaction pathways without altering the overall reaction process.

Key principle for constructing the nitrogen-source differentiation is to ensure that simulation results from the new mechanism remain entirely consistent with those from the original, undifferentiated mechanism. Specifically, this differentiation must preserve all inherent reaction pathways. To achieve this, the new method ensure that the consumption and formation rates of every species involved in each elementary reaction remain unchanged. Maintaining the net reaction rate of each species in each reaction step at any given moment ensures accurate computation throughout the entire reaction process.

Based on the ammonia combustion reaction mechanism developed by Zhang et al. [47], this study constructs a new reaction mechanism capable of identifying nitrogen elements. Table 1 illustrates the composition of nitrogen-containing reactants before and after the

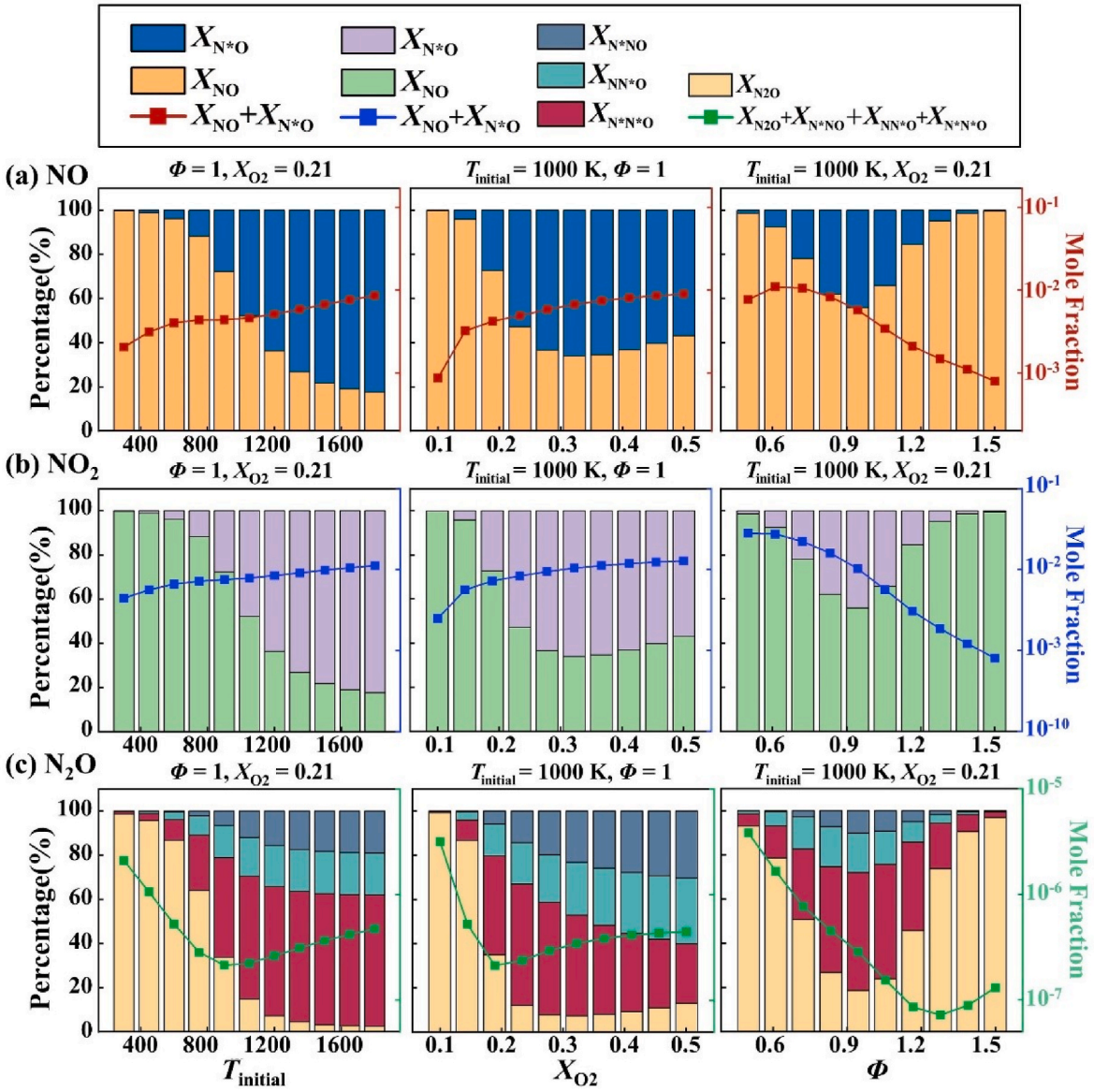

Fig. 3. Proportion of NO_x from NH_3-sourced (NO_x) and N*N*-sourced (N*O_x) with different $T_{initial}$, X_{O2} and Φ, with mole fraction also presented.

differentiation process. Notably, for rotational asymmetrical nitrogen components (e.g., N_2O, NNH), the position of each nitrogen atom must be considered, which is often neglected in previous studies.

This research also addresses the impact of labeling nitrogen positions in the differentiation of multi-nitrogen substances with rotational asymmetric. For example, in the reaction containing N_2O:

$$N + NO_2 \leftrightarrow N_2O + O \quad \text{(R4)}$$

The nitrogen identification should consider the position of nitrogen relative to oxygen, with only one nitrogen atom labeled, i.e.,

$$N^* + NO_2 \leftrightarrow N^*NO + O \quad \text{(R5)}$$

$$N + N^*O_2 \leftrightarrow NN^*O + O \quad \text{(R6)}$$

This division aligns with the principles for establishing elementary reactions. Similar considerations apply to other components such as NNH and N_2H_3.

Before outlining the approach, it is important to first explain the computational methods employed for elementary reactions in the numerical simulations. For reversible reactions such as

$$A + B \leftrightarrow C + D \quad \text{(R7)}$$

the forward and reverse reaction rates are respectively expressed as follows [48]:

$$r_f = k_f[A][B] \quad (1)$$

$$r_r = k_r[C][D] \quad (2)$$

And the net reaction rate of reactant A is:

$$\frac{d[A]}{dt} = k_f[A][B] - k_r[C][D] \quad (3)$$

In the above, r_f and r_r represent the forward and reverse reaction rates, while k_f and k_r are the reaction rate constants for the forward and reverse reactions, respectively; [X] denotes the mole concentration of component X. The reaction rate constants are calculated using the Arrhenius equation. Specific cases are discussed below, with detailed reaction examples from Zhang et al.'s mechanism [47] provided in Table 2:

Case (i). reactant A and product C both contain nitrogen elements

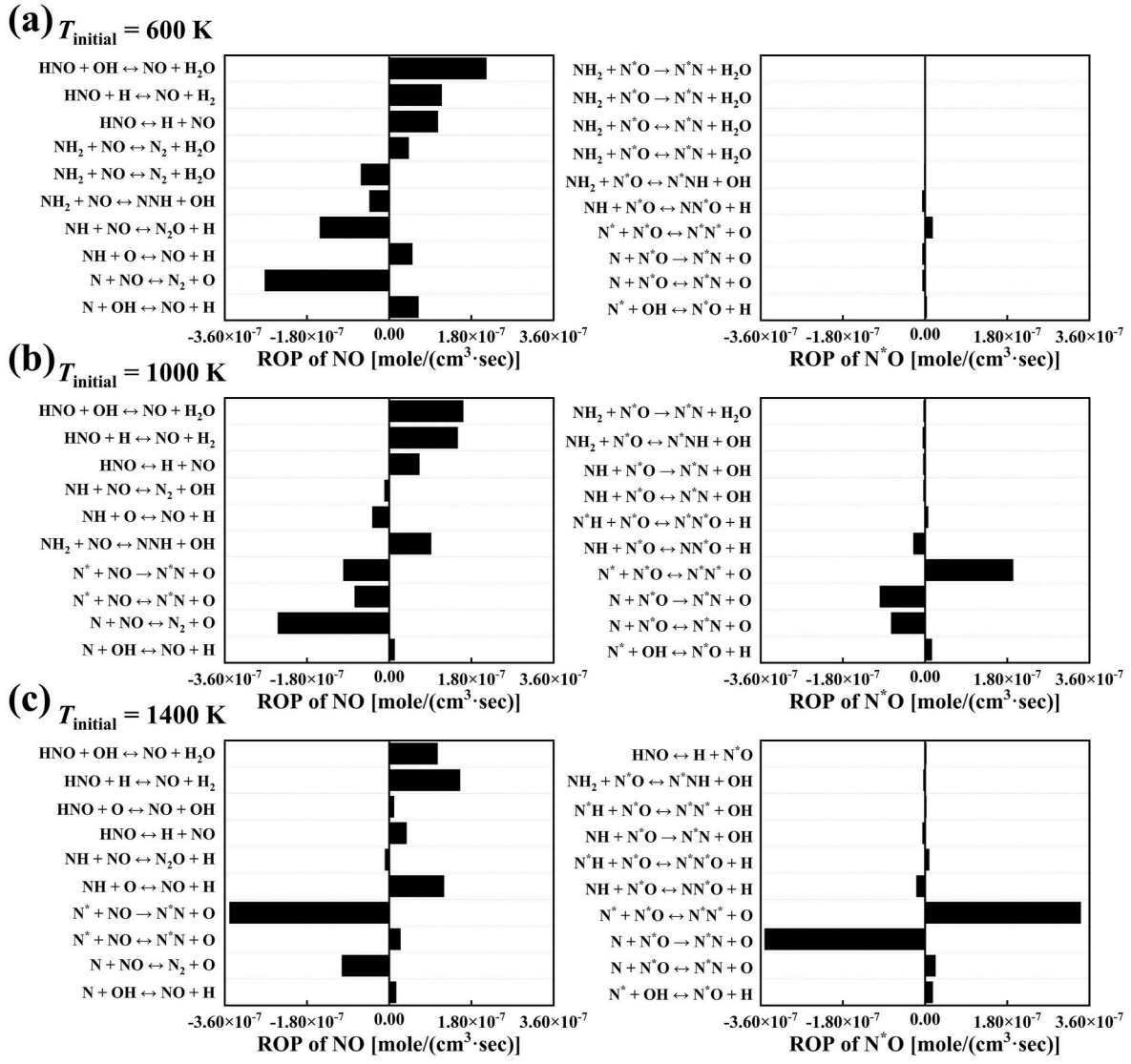

Fig. 4. Rates of production (ROP) of NO/N*O for the top 10 reactions during $NH_3/O_2/N^*N^*$ combustion in PSR at $\Phi = 1.0$, $X_{O2} = 0.21$, and $T_{initial}$ of (a) 600 K, (b) 1000 K, (c) 1400 K.

Assume that both A and C contain one nitrogen atom each. In this case, A can be divided into two components, A_1 and A*, representing different nitrogen sources. A similar division applies to C. The reaction is then divided into two sub-reactions:

$$A_1 + B \leftrightarrow C_1 + D \tag{R8}$$

$$A^* + B \leftrightarrow C^* + D \tag{R9}$$

The forward and reverse reaction constants k_f and k_f remain consistent, preserving the total reaction rate:

$$\frac{d[A_1 + A^*]}{dt} = k_f([A_1] + [A^*])[B] - k_r([C_1] + [C^*])[D] = k_f[A][B] - k_r[C][D] = \frac{d[A]}{dt} \tag{4}$$

Similarly,

$$\frac{d[B_1 + B^*]}{dt} = k_f([A_1] + [A^*])[B] - k_r([C_1] + [C^*])[D] = \frac{d[B]}{dt} \tag{5}$$

$$\frac{d[C_1 + C^*]}{dt} = k_r([C_1] + [C^*])[D] - k_f([A_1] + [A^*])[B] = \frac{d[C]}{dt} \tag{6}$$

$$\frac{d[D_1 + D^*]}{dt} = k_r([C_1] + [C^*])[D] - k_f([A_1] + [A^*])[B] = \frac{d[D]}{dt} \tag{7}$$

If A contains more than one nitrogen atom, this principle applies similarly, ensuring that the reaction constants remain the same for each pathway.

Case (ii). both reactants contain nitrogen elements

If both A and B contain nitrogen, reaction R7 should be divided into four sub-reactions:

$$A_1 + B_1 \leftrightarrow C_1 + D_1 \tag{R10}$$

$$A_1 + B^* \leftrightarrow C_1 + D^* \tag{R11}$$

$$A^* + B_1 \leftrightarrow C^* + D_1 \tag{R12}$$

$$A^* + B^* \leftrightarrow C^* + D^* \tag{R13}$$

The reaction constants for the above reactions should also be k_f and k_r to ensure the total reaction rate unchanged:

Table 3
Correlation pathways for NH_3-Sourced NO and N*N*-Sourced N*O production and consumption.

NH_3-Sourced [36]			
Extened Zeldovich	R45 $N + O_2 \leftrightarrow NO + O$	R47 $N + OH \leftrightarrow NO + H$	R49 $N + NO \leftrightarrow N_2 + O$
	R50 $N^* + NO \leftrightarrow N^*N + O$	R52 $N^* + NO \rightarrow N^*N + O$	
HNO	R714 $HNO \leftrightarrow H + NO$	R716 $HNO + O \leftrightarrow NO + OH$	R718 $HNO + H \leftrightarrow NO + H_2$
	R720 $HNO + OH \leftrightarrow NO + H_2O$	R722 $HNO + O_2 \leftrightarrow NO + HO_2$	R762 $NO + OH(+M) \leftrightarrow HONO(+M)$
NH_i	R57 $NH + O \leftrightarrow NO + H$	R67 $NH + O_2 \leftrightarrow NO + OH$	R686 $NNH + O \leftrightarrow NH + NO$
	R688 $NN^*H + O \leftrightarrow N^*H + NO$		
DeNO$_x$	R81 $NH + NO \leftrightarrow N_2O + H$	R82 $N^*H + NO \leftrightarrow N^*NO + H$	R85 $NH + NO \leftrightarrow N_2 + OH$
	R86 $N^*H + NO \leftrightarrow N^*N + OH$	R88 $N^*H + NO \rightarrow N^*N + OH$	R141 $NH_2 + NO \leftrightarrow NNH + OH$
	R142 $N^*H_2 + NO \leftrightarrow NN^*H + OH$	R145 $NH_2 + NO \leftrightarrow N_2 + H_2O$	R146 $NH_2 + NO \leftrightarrow N_2 + H_2O$
NO$_{undefined}$	R764 $NO + HO_2 \leftrightarrow NO_2 + OH$	R770 $NO_2 + H \leftrightarrow NO + OH$	R774 $NO + O(+M) \leftrightarrow NO_2(+M)$
	R798 $N^*NO + O \leftrightarrow N^*O + NO$	R799 $NN^*O + O \rightarrow N^*O + NO$	
N*N*-sourced [22]			
Thermal	R46 $N^* + O_2 \leftrightarrow N^*O + O$	R48 $N^* + OH \leftrightarrow N^*O + H$	R51 $N + N^*O \leftrightarrow N^*N + O$
	R53 $N + N^*O \rightarrow N^*N + O$	R54 $N^* + N^*O \leftrightarrow N^*N^* + O$	
N_2O-intermediate	R83 $NH + N^*O \leftrightarrow NN^*O + H$	R84 $N^*H + N^*O \leftrightarrow N^*N^*O + H$	R798 $N^*NO + O \leftrightarrow N^*O + NO$
	R799 $N^*NO + O \rightarrow N^*O + NO$	R800 $N^*N^*O + O \leftrightarrow 2N^*O$	
NNH	R687 $N^*NH + O \leftrightarrow NH + N^*O$	R689 $N^*N^*H + O \leftrightarrow N^*H + N^*O$	R719 $HN^*O + H \leftrightarrow N^*O + H_2$
	R721 $HN^*O + OH \leftrightarrow N^*O + H_2O$		
NO-reburning	R87 $NH + N^*O \leftrightarrow N^*N + OH$	R89 $NH + N^*O \rightarrow N^*N + OH$	R90 $N^*H + N^*O \leftrightarrow N^*N^* + OH$
	R149 $NH_2 + N^*O \leftrightarrow N^*N + H_2O$	R150 $NH_2 + N^*O \leftrightarrow N^*N + H_2O$	R153 $NH_2 + N^*O \rightarrow N^*N + H_2O$
	R154 $NH_2 + N^*O \rightarrow N^*N + H_2O$		
N*O$_{undefined}$	R58 $N^*H + O \leftrightarrow N^*O + H$	R143 $NH_2 + N^*O \leftrightarrow N^*NH + OH$	R715 $HN^*O \leftrightarrow H + N^*O$
	R765 $N^*O + HO_2 \leftrightarrow N^*O_2 + OH$	R771 $N^*O_2 + H \leftrightarrow N^*O + OH$	R775 $N^*O + O(+M) \leftrightarrow N^*O_2(+M)$

$$\frac{d[A_1 + A^*]}{dt} = k_f([A_1] + [A^*])([B_1] + [B^*]) - k_r([C_1] + [C^*])([D_1] + [D^*])$$

$$= k_f[A][B] - k_r[C][D] = \frac{d[A]}{dt} \tag{8}$$

$$\frac{d[C_1 + C^*]}{dt} = k_r([C_1] + [C^*])([D_1] + [D^*]) - k_f([A_1] + [A^*])([B_1] + [B^*]) = \frac{d[C]}{dt} \tag{9}$$

Similarly, the products follow the same derivation. When A and B contain more nitrogen atoms, the division of reactions follows the same process.

Case (iii). A and B are the same substance

(1) Producing two different species C and D

$$A + A \leftrightarrow C + D \tag{R14}$$

Assume that A contains a single nitrogen atom, and both C and D contain nitrogen atoms. The reaction should be divided into sub-reactions which contain duplicate reactions which are irreversible:

$$A_1 + A_1 \leftrightarrow C_1 + D_1 \tag{R15}$$

$$A^* + A_1 \leftrightarrow C^* + D_1 \tag{R16}$$

$$A^* + A_1 \rightarrow C^* + D_1 \tag{R17}$$

$$A^* + A_1 \leftrightarrow C_1 + D^* \tag{R18}$$

$$A^* + A_1 \rightarrow C_1 + D^* \tag{R19}$$

$$A^* + A^* \leftrightarrow C^* + D^* \tag{R20}$$

The forward and reverse reaction rate constants should be k_f and k_r to ensure the net reaction rate remains unchanged:

$$\frac{d[A_1 + A^*]}{dt} = 2k_f[A_1]^2 + 2k_f[A^*]^2 + 4k_f[A_1][A^*] - k_r[C_1][D_1] - k_r[C_1][D^*]$$

$$-k_r[C^*][D_1] - k_r[C^*][D^*] = 2k_f[A]^2 - k_r[C][D] = \frac{d[A]}{dt} \tag{10}$$

$$\frac{d[C_1 + C^*]}{dt} = k_r[C_1][D_1] + k_r[C_1][D^*] + k_r[C^*][D_1] + k_r[C^*][D^*] - 2k_f[A_1]^2 - 2k_f[A^*]^2$$

$$-4k_f[A_1][A^*] = k_r[C][D] - 2k_f[A]^2 = \frac{d[C]}{dt} \tag{11}$$

(2) Producing only one product C, with A containing only one nitrogen atom:

$$A + A \leftrightarrow C \tag{R21}$$

The reaction is divided into:

$$A_1 + A_1 \leftrightarrow C_{11} \tag{R22}$$

$$A^* + A_1 \leftrightarrow C_1{}^* \tag{R23}$$

$$A^* + A_1 \rightarrow C_1{}^* \tag{R24}$$

$$A^* + A^* \leftrightarrow C^{**} \tag{R25}$$

The forward rate constants for R22, R23, R24, and R25 are set as k_f, k_f, 3 k_f, and k_f, respectively, with the reverse rate constant k_r unchanged, to preserve the overall reaction rate after dividing:

$$\frac{d[A_1 + A^*]}{dt} = 2k_f[A_1]^2 + 2k_f[A^*]^2 + 4k_f[A_1][A^*] - k_r([C_{11}] + [C_1{}^*] + [C^{**}])$$

$$= 2k_f[A]^2 - k_r([C]) = \frac{d[A]}{dt} \tag{12}$$

$$\frac{d[C_{11} + C_1{}^* + C^{**}]}{dt} = k_r([C_{11}] + [C_1{}^*] + [C^{**}]) - 2k_f[A]^2 = k_r[C] - 2k_f[A]^2 = \frac{d[C]}{dt} \tag{13}$$

For cases where A contains more than one nitrogen atom, the same method applies, ensuring that the net reaction rate is maintained.

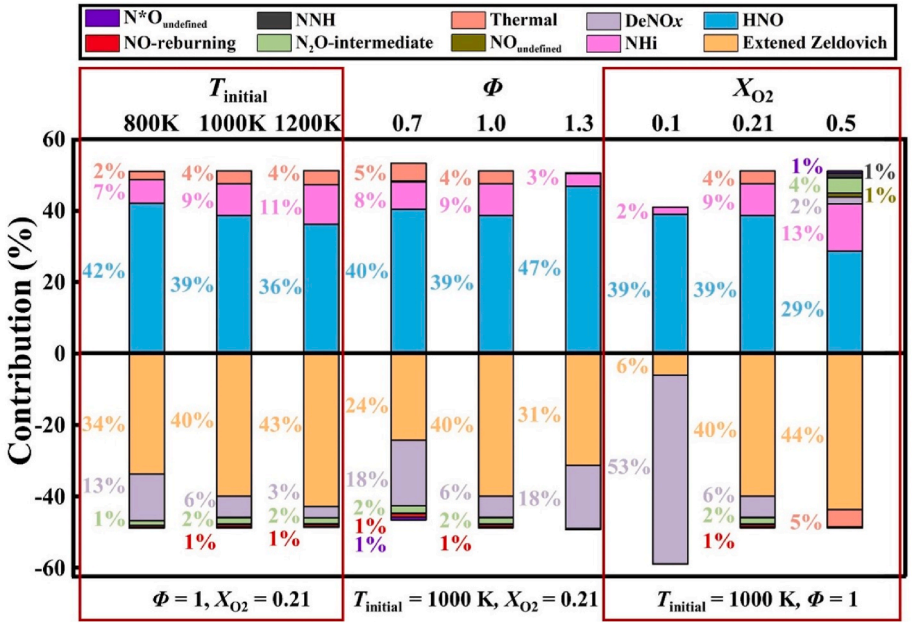

Fig. 5. Contribution of NO_{total}(NO + N*O) production pathways in $NH_3/O_2/N_2$ systems under different $T_{initial}$, X_{O2}, and Φ (NO_x and $N*O_x$).

Case (iv). reactions involve three-body collisions

$$A + B + (M) \leftrightarrow C + D + (M) \quad \text{(R26)}$$

In this case, a third body M is involved, its effect is reflected in the rate of progress variable [49]:

$$q_i = \left(\sum_{n=1}^{N} (a_{ni})[X_n] \right) \left(k_{fi}[A][B] - k_{ri}[A][B] \right) \quad (14)$$

Here, X_n is the coefficient of the third body component n, k_{fi} is the forward reaction constant, and k_{ri} is the reverse reaction constant. The presence of a third body does not alter the overall chemical reaction equations, and the nitrogen-containing species are unaffected by the differentiation process. Pressure-dependent reactions [50,51] can be handled similarly. In this context, the reaction can be reformulated using the general approach outlined above.

Following this methodology, the detailed NH_3 combustion mechanism proposed by Zhang et al. [47] is applied to build a new mechanism. After incorporating nitrogen differentiation, the original mechanism, which consists of 38 species and 263 reactions, is expanded to include 74 species and 946 reactions. A comprehensive description of the new mechanism, as well as the CHEMKIN format data can be found in the Supplementary Materials.

More generally, this method is applicable for identifying various elements present in both the fuel and oxidizer. In the Supplementary Materials, the study present simulation error results for a CH_4–CO_2 system based on the GRI-3.0 mechanism [47,52], after identifying the carbon sources, as well as its CHEMKIN format files.

For the kinetic studies, a zero-dimensional perfectly-stirred-reactor (PSR) are employed. These models simulate constant-volume, constant-mass, adiabatic systems, where the fuel and oxidizer are fully mixed prior to the reaction, thus isolating the effects of mixing, convection, and radiation. The residence time is set at 1.0 s. In this work, the fuel is denoted as NH_3, and the oxidizer is a mixture of O_2 and N_2(N*N*), with mole fractions ranging from 0.1 to 0.5 for O_2 and 0.9 to 0.5 for N_2(N*N*), and the equivalence ratio is varied between 0.7 and 1.3.

3. Results and discussion

3.1. Validation of the reaction mechanism based on nitrogen source identification

This study first present whether the simulation results keep unchanged after using the nitrogen source differentiation method, thereby confirming the validity of the proposed approach. Fig. 1 illustrates the oxidation processes simulated in PSR under two conditions: one without nitrogen source identification ($NH_3/N_2/O_2$) and one with nitrogen source identification ($NH_3/N*N*/O_2$). The initial conditions are set to $T_{initial} = 1600$ K, $X_{O2} = 0.21$, and $\Phi = 1$. The "Total" value represents the mole fraction of species derived from both NH_3 and N_2(N*N*). The results show a high degree of similarity between both cases, with a maximum relative error of only 0.00793 % in the peak species mole fractions. Specifically, the errors for NO, NO_2, and N_2O are 0.000114 %, 0.00793 %, and 0.00102 %, respectively, indicating that nitrogen differentiation has a negligible effect on species conversion.

Fig. 2 presents the rate of production (ROP) for NH_3 combustion in the PSR under the same initial conditions ($T_{initial} = 1600$ K, $X_{O2} = 0.21$, and $\Phi = 1$). The ROP values are compared for cases with nitrogen source identification ($NH_3/N*N*/O_2$) and without nitrogen source identification ($NH_3/N_2/O_2$). The ROP values show strong consistency, with a maximum relative error of 0.612 %. The specific ROP errors for NO, NO_2, and N_2O are 0.0036 %, 0.0147 %, and 0.00908 %, respectively, further validating the accuracy of the nitrogen differentiation mechanism in modeling combustion reactions.

Moreover, the average relative errors for peak and equilibrium concentrations, as well as maximum ROP values for key species under varying conditions, including $T_{initial}$ (1200 K, 1600 K, 2000 K), X_{O2} (0.1, 0.21, 0.5), and Φ (0.5, 1, 2), were also evaluated. Across all conditions, the maximum mole fractions of most components exhibit relative errors below 0.1 %, which can be considered computational error. For equilibrium states, the average errors for NO, NO_2, and N_2O are 0.277 %, 0.139 %, and 0.000 %, respectively. These results confirm that the new mechanism accurately reproduces chemical equilibrium states and ensures reliable emission predictions. The ROP errors for other species involved in the mechanism, as well as the average relative errors for peak and equilibrium concentrations, are provided in the Supplementary Materials.

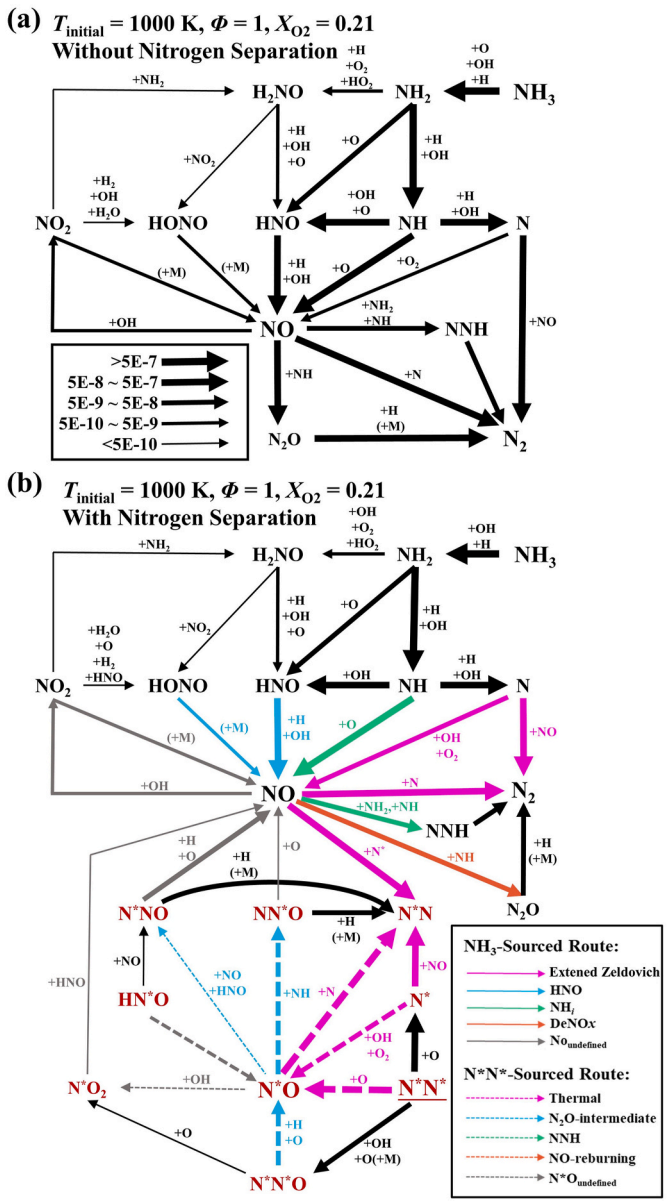

Fig. 6. Oxidation pathways for homogeneous rector simulation at $T_{initial}$ = 1000 K, X_{O2} = 0.21, and Φ = 1 with nitrogen source identification (NH_3/N*N*/O_2).

3.2. NO_x generation of NH_3 combustion under different conditions

Fig. 3 illustrates the mole fractions of NO_x in PSR system under varying inlet temperatures ($T_{initial}$), oxygen concentrations (X_{O2}), and equivalence ratios (Φ). The figure also differentiates the contributions of nitrogen oxides from NH_3 and N*N*-derived species. In Fig. 3a, the total mole fraction of NO increases steadily with rising $T_{initial}$. Notably, the proportion of NO derived from N_2 increases sharply, reaching approximately 0.4 at 1000 K and nearly 0.8 at 1500 K. This shift marks a transition in the dominant source of NO_x from NH_3-derived to N*N*-derived. This temperature range represents a critical transition point in the NO_x formation pathways. As X_{O2} increases, total NO production rises gradually. However, the proportion of N*O initially increases rapidly before declining. This behavior is influenced by the dual effects of oxygen concentration on combustion temperature: at lower oxygen levels, higher temperatures favor the formation of thermal NO from N*N*. At higher X_{O2}, the decreasing mole fraction of N*N* becomes the dominant factor, reducing N*O production from N*N*. When Φ varies between 0.5 and 1.5, the proportion of N*O reach its peak value at Φ = 1. This previously unaddressed trend underscores the importance of further research to better understand the combined effects of equivalence ratio on different nitrogen oxide pathways.

Fig. 3b and c depict the mole fraction ratios of NO_2 to NO under varying $T_{initial}$, X_{O2}, and Φ. Overall, the trends for NO_2 and N_2O nitrogen sources are similar to those of NO, although their total mole fractions are significantly lower. Notably, the differences in the contributions of N*NO and NN*O highlight the complexity of NH_3–N*N* interactions during N_2O formation, underscoring the need for further investigation into the mechanisms of NO_x generation in ammonia combustion. Moreover, these results validate the optimization method proposed by Wu et al. [46], confirming the necessity of considering both the symmetry and asymmetry of multi-nitrogen atom components in the mechanism for distinguishing nitrogen species.

Fig. 4 illustrates the rate of production (ROP) of NO/N*O via key reactions at initial temperatures ($T_{initial}$) of 600 K, 1000 K, and 1400 K, with an oxidizer mole fraction (X_{O2}) of 0.21 and an equivalence ratio (Φ) of 1.0. As clearly shown in the figure, the dominance of N_2-derived NO_x formation pathways at higher temperatures can be attributed to two main factors:

(i) With increasing $T_{initial}$, the N_2-derived pathway, particularly the Zeldovich route (N*N* + O ↔ N* + N*O), is significantly enhanced, producing abundant NO.
(ii) Simultaneously, N* radicals formed with N*O through Zeldovich route substantial NO consumption via the reaction N* + NO → N*N + O, thus reducing the net NO concentration in the combustion products.

Regarding NH_3-derived NO_x formation, as temperature increases, NO formation through the HNO-intermediate route diminishes, while NH_i pathway NH + O ↔ NO + H become increasingly prominent. This shift occurs because higher temperatures promote OH radicals convert into H and O (e.g., OH + OH ↔ O + H_2O, OH + H_2 ↔ H + H_2O), thereby inhibiting the HNO + OH → NO + H_2O pathway. Detailed discussion regarding the rates of production (ROP) for NO as a function of X_{O2} and Φ, and N_2O as a function of $T_{initial}$, X_{O2} and Φ is provided in the Supplementary Materials.

Table 3 outlines the primary reaction pathways contributing to NO formation from NH_3 and N_2 under various conditions $T_{initial} \in$ [800–1000] K, $X_{O2} \in$[0.1–0.5], $\Phi \in$[0.5–1]. The table presents the top 20 reactions, ranked by their net generation and consumption rates for each simulation. The results clearly demonstrate the successful identification of NO_x formation mechanisms originating from NH_3 and N*N*. Interestingly, the table reveals that intermediates originating from NH_3 and N*N* can also participate in pathways typically associated with the other nitrogen source, as can be named as "N–N* interaction" reactions. These cross-pathway interactions highlight a previously unreported dynamic in ammonia combustion, where nitrogen species transition between source-dependent mechanisms, suggesting a more complex interplay than previously understood.

Fig. 5 presents the relative contributions of various reaction pathways to NO_{total} formation in the NH_3/O_2/N*N* system under different conditions of $T_{initial}$, X_{O2}, and Φ, contributions of less than 1% are recorded as 0. These contributions are calculated as the proportion of each pathway's net reaction rate to NO_{total} reaction rate under the conditions of $T_{initial} \in$ [800 – 1000] K, $X_{O2} \in$[0.1 – 0.5], $\Phi \in$[0.5 – 1]. Across all conditions, NH_3-derived NO dominate, while the generation and consumption rates of N*O remain relatively low. Notably, the Extend Zeldovich pathway for NH_3-derived NO is the primary consumption route, transitioning to $DeNO_x$ pathways only under low oxygen concentrations (0.1), consistent with Liu et al. [22].

At elevated temperatures, NH_3-derived pathways involving NH_i intermediates become more significant, while the contributions of HNO

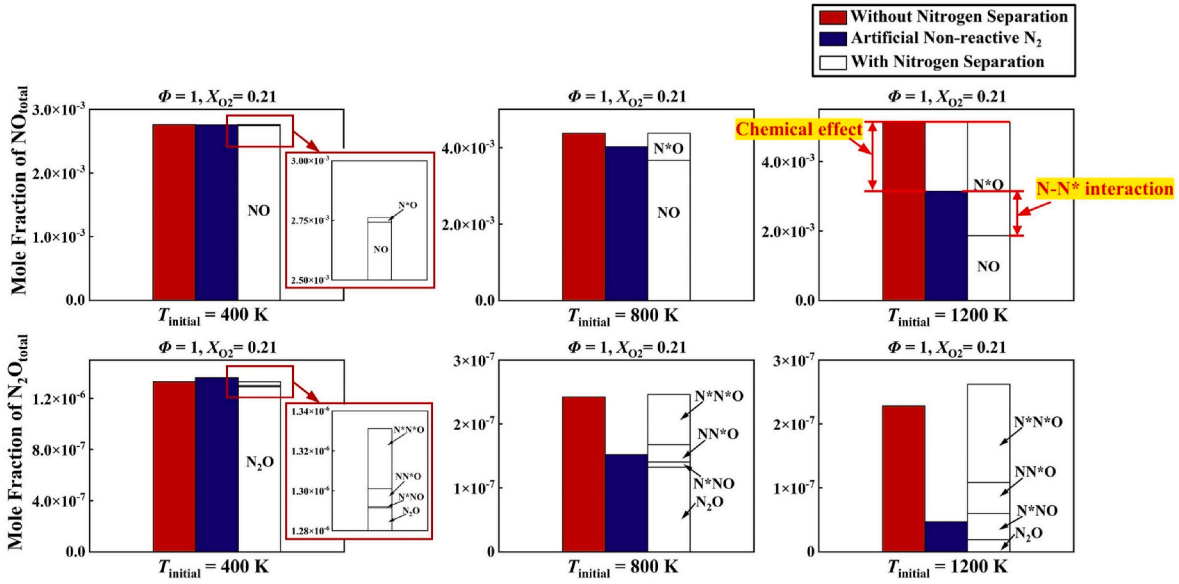

Fig. 7. NO and N_2O production under different $T_{initial}$, X_{O2}, and Φ using three mechanisms: without & with nitrogen differentiation, and with artificial species (FN_2).

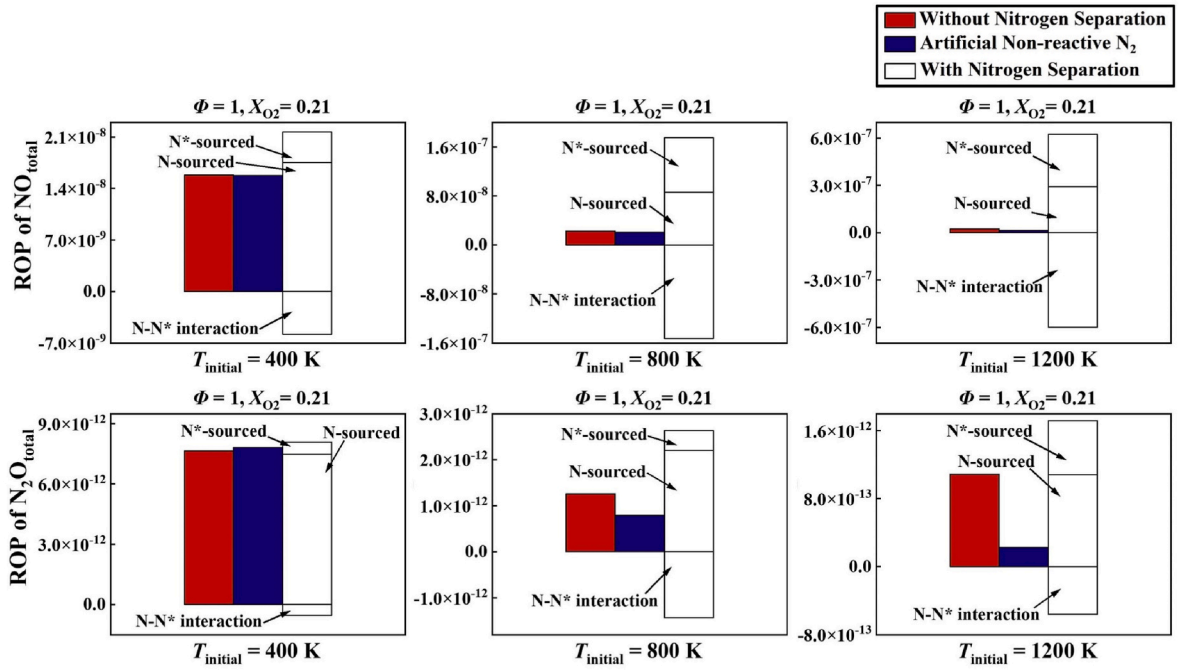

Fig. 8. Rate of product (ROP) of NO and N_2O under different $T_{initial}$, X_{O2}, and Φ using three mechanisms: without & with nitrogen differentiation, and with artificial species (FN_2).

and $DeNO_x$ pathways decrease. For N*N*-derived N*O, the thermal route's contribution steadily increases with temperature. Among the reduction pathways, N_2O intermediates and NO reburning play dominant roles for N*O. The equivalence ratio (Φ) also exerts a significant influence on NO generation. Specifically, the contribution of the HNO pathway initially decreases but then increases as Φ shifts from lean to rich conditions. For NO consumption, the Extended Zeldovich pathway sharply increases before declining, while the $DeNO_x$ pathway follows the opposite trend. These variations are driven by changes in O and O_2 concentrations as Φ shifts [33,34]. Higher Φ values near 1 increase combustion temperatures due to reduced heat capacity, enhancing O formation. This suppresses HNO production and shifts the balance between $DeNO_x$ and NH_i pathways.

Similarly, as X_{O2} increases, the dominant NO consumption pathway transitions from $DeNO_x$ to the Extended Zeldovich pathway, while NO generation pathways evolve from being primarily HNO-driven to more intricate combinations. These findings underscore the intricate interplay of oxygen concentration, equivalence ratio, and nitrogen oxide formation and consumption dynamics in ammonia combustion. The analysis highlights the complexity of NO_x formation in ammonia combustion and calls for further research to elucidate the interactions between various pathways and develop effective NO_x emission control strategies.

Fig. 6 illustrates the oxidation pathways in PSR simulated under conditions of $T_{initial} = 1000$ K, $X_{O2} = 0.21$, and $\Phi = 1$ using mechanisms with and without nitrogen source identification. The newly developed mechanism effectively distinguishes between NH_3-sourced and N*N*-

sourced nitrogen oxides, offering a robust framework for identifying NO formation sources. Additionally, it explicitly captures the interactions between intermediates derived from NH_3 and N*N*, such as NO → N*N and N*O → N*N*. These findings emphasize the need to reassess NO_x generation mechanisms in ammonia combustion to account for these complex interactions. Furthermore, Fig. 6b clearly shows that the generation and consumption pathways of N*NO and NN*O are distinctly different, underscoring the necessity and validity of the optimization method of Wu et al. [46] in this study.

3.3. Comparison with the artificial species method

Fig. 7 compares production of NO/N*O and N_2O/N*N*O/N*NO/NN*O production under varying $T_{initial}$, X_{O2}, and Φ using three mechanisms: without nitrogen source identification, with nitrogen source identification, and with artificial species (FN_2) that lack chemical reactivity. Notably, the mechanism employing FN_2 exhibits significant deviations in NO production compared to the nitrogen differentiation mechanism. This discrepancy arises due to two distinct chemical effects of N_2 on NO formation: (i) N_2 directly contributes to NO formation through reaction pathways involving N_2-derived species, and (ii) N_2-derived intermediates interact with NH_3-derived intermediates, influencing NO production. The FN_2 approach cannot distinguish between these two effects of N_2. However, the nitrogen source identification method proposed in this study clearly isolates the second effect, specifically the reduction in NO mole fraction attributed to N*N*, facilitating a more detailed investigation of NO_x formation mechanisms from various sources and pathways in ammonia combustion.

Furthermore, analysis of reaction temperature changes reveals the following trends: (i) as temperature increases, the chemical effect of N_2 becomes more prominent in the FN_2 approach, indicating activation of reactions involving N*N*; (ii) the proportion of NO gradually increases with rising temperature; and (iii) the interaction between NH_3 and N_2 intensifies, accompanied by a similar trend in N_2O production. These trends can be attributed to high temperatures enhancing the activation of the N*N* pathway, resulting in a significant increase in N* intermediates that participate in combustion reactions. This behavior is also observed for N_2O. Consequently, the chemical effect of N* becomes increasingly significant in high-temperature combustion, underscoring the need for systematic investigation to fully elucidate this complex process.

Fig. 8 illustrates the net reaction rates of NO and N_2O simulated using three different reaction mechanisms under varying initial reactant temperatures. The reactions are categorized into three groups based on the chemical effects of N*N*: (i) reactions originating from N*N*, (ii) reactions originating from NH_3, and (iii) reactions involving interactions between N* and N. The present nitrogen source identification mechanism effectively separates the reaction rates for each source, highlighting the contributions of each pathway to the overall process. As shown in Fig. 8, the NO production rate from N*-derived reactions increases with temperature, while interactions between NH_3 and N*N* become more significant. Moreover, the N–N* interaction consistently serves as the consumption path for NO_x, even in low temperature case. Therefore, such N–N* interaction should be carefully considered in low NO_x control strategies. These findings highlight the crucial role of N*N*-derived reactions in both NH_3 combustion. The rise in temperature enhances the activity of N*N*-derived reactions, which significantly influence the NH_3 combustion process—an effect not previously identified in prior studies.

In conjunction with the findings from Fig. 7, it is evident that the interaction between NH_3 and N*N* plays an important role in NO production during combustion. Specifically, NO formation predominantly follows NH_3-derived pathways, but these are strongly influenced by N*N*. This highlights the significant coupling between NH_3- and N*N*-derived species in NO formation. Notably, the artificial FN_2 method fails to capture the critical impact of N*N* interactions, emphasizing the need for this nitrogen source identification method.

In summary, by identifying between NH_3- and N_2-derived nitrogen species, the proposed approach effectively differentiate their respective contributions to NO_x formation, providing a novel framework for understanding the complex mechanisms of NO_x formation in ammonia combustion. Furthermore, integrating the artificial species method allows for a clearer differentiation of the two chemical effects of N_2 on NO formation: (i) direct NO production via N_2-derived pathways and (ii) the influence of N_2-derived intermediates on NH_3-derived NO pathways, which is defined as "N–N* interaction" in the present work. This interactions between NH_3 and N*N* species during combustion are discovered not only significant but also increasingly pronounced as temperature rises. These results underscore the indispensable role of N*N* (or N_2)-derived species in NO formation during combustion and highlight the necessity of systematic investigation into these interactions.

The strengthened interactions between N and N* species are clearly illustrated in Fig. 4. At an initial reactant temperature of 600 K, the primary NO consumption reactions include $N + NO \leftrightarrow N_2 + O$ and $NH + NO \leftrightarrow N_2O + H$. However, as the initial temperature increases, reactions involving coupled N–N* interactions, specifically $N^* + NO \leftrightarrow N^*N + O$ and $N + N^*O \leftrightarrow N^*N + O$, become progressively more significant. By an initial temperature of 1400 K, these coupled reactions dominate NO consumption.

It is noteworthy that rising temperatures enhance the thermal pathway of NN via the reaction $N^*N^* + O \leftrightarrow N^*O + N^*$, producing abundant N* radicals, which in turn substantially promote NO consumption through the aforementioned coupling reactions. This mechanism, clearly illustrated in Fig. 5, highlights how N–N* interactions significantly reduce the net NO concentration. Furthermore, around 800 K, as depicted in Fig. 3, a slight reduction in total NO formation occurs despite the concurrent promotion of thermal NO formation. This observation can be attributed to the enhanced thermal formation of N*N*, which subsequently accelerates the coupled NO consumption reactions ($N^* + NO \leftrightarrow N^*N + O$ and $N + N^*O \leftrightarrow N^*N + O$). Although the thermal pathways substantially generate NO, the NO/N*O consumption effect by N/N* radicals remain pronounced—a crucial finding not identified in previous studies.

These results underline the importance of appropriately controlling the spatial distribution of N*N* species, particularly within high-temperature reaction zones, to effectively suppress fuel-derived NO formation and limit thermal N*O generation during ammonia combustion.

4. Conclusions

Ammonia (NH_3) is a promising zero-carbon fuel with significant potential for reducing greenhouse gas emissions. However, its application is hindered by the substantial formation of nitrogen oxides (NO_x) during combustion, which poses a major environmental challenge. A critical issue in understanding NO_x formation lies in the overlapping reaction pathways of NH_3 and N_2, both of which contribute to NO_x production. To address this, the present study has refined the nitrogen source identification method proposed by Wu et al. [46], enabling a precise distinction between NH_3- and N_2-derived reactions without altering the overall combustion process. This method allows for the accurate identification of nitrogen species, particularly capturing the effects of rotational asymmetry in multi-nitrogen atom structures, and provides comprehensive guidelines for decomposing reaction equations under a wide range of combustion conditions. The newly constructed mechanism based on this method facilitates a clear identification of NO_x formation pathways and provides valuable insights into the contributions of each nitrogen source. The key findings are as follows:

(1) The combustion process remains unchanged with nitrogen source identification. The mechanism developed using nitrogen

differentiation produces results nearly identical to these by the original mechanism, with a maximum error in mole fractions of less than 0.07 % and species reaction rate errors below 0.612 %. Moreover, the prediction error of rotationally asymmetric multi-nitrogen atom species is significantly reduced, as the prediction error of N_2O is reduced to 1/10 compared with the mechanism that ignore such asymmetric.

(2) The mechanism effectively distinguishes NO_x formation from NH_3- and N_2-derived nitrogen sources. It also uncovers interactions where nitrogen species transition between pathways typically associated with the other source. Comparisons with the artificial species (FN_2) method quantitatively demonstrate the distinct contributions of NH_3 and N_2 to NO formation. Moreover, the interaction between NH_3 and N_2 is observed very important for NH_3 combustion, especially at higher temperature. Additionally, the distinct concentration and transformation pathways of N*NO and NN*O—products of asymmetric multi-nitrogen atom interactions—highlight the necessity of further refining the nitrogen differentiation method.

(3) Analysis of temperature ($T_{initial}$), oxygen concentration (X_{O2}), and equivalence ratio (Φ) revealed significant transitions in NO_x formation pathways. At higher temperatures, NH_3-derived NO formation shifts toward N_2-derived pathways. Variations in X_{O2} and Φ also highlight the dynamic of NO_x generation, emphasizing the need for further research into the interplay of these factors.

(4) The present method, combined with the artificial species approach, quantitatively reveals the chemical effects of N*N* on NO_x formation. These effects become increasingly significant as temperature rises. Moreover, the N–N* interaction is a primary NO consumption pathway during combustion through N* + NO → N*N + O and N + N*O → N*N + O.

(5) In future studies, the aforementioned nitrogen-source differentiation mechanism will be utilized to further elucidate complex elemental transformations and interactions during combustion. Additionally, the significance of N–N* interactions in reaction kinetics simulations on NO_x formation and reduction in practical combustion should also be validated.

In conclusion, the newly developed mechanism successfully distinguishes NH_3- and N_2-sourced NO_x formation while maintaining computational accuracy. This approach offers a robust framework for understanding the complex pathways of NO_x formation during ammonia combustion. Future research will focus on further exploring the intricate NO_x generation mechanisms and optimizing this differentiation method for broader applications.

CRediT authorship contribution statement

Shuang Li: Writing – review & editing, Writing – original draft, Visualization, Validation, Software, Methodology, Investigation, Formal analysis, Data curation, Conceptualization. **Jicang Si:** Writing – review & editing, Supervision, Resources, Funding acquisition, Conceptualization. **Xiangtao Liu:** Writing – review & editing, Investigation. **Yuanye Guo:** Writing – review & editing. **Guochang Wang:** Writing – review & editing, Supervision, Funding acquisition. **Enguang Xu:** Writing – review & editing. **Jialin Zou:** Writing – review & editing. **Qiuhao Zhang:** Writing – review & editing. **Minyi Xu:** Writing – review & editing, Supervision. **Jianchun Mi:** Writing – review & editing, Supervision, Funding acquisition.

Declaration of competing interest

The authors declare that they have no known competing financial interests or personal relationships that could have appeared to influence the work reported in this paper.

5. Acknowledgements

The authors gratefully acknowledge the supports of the National Natural Science Foundation of China (No. 2231101929 & 22350710788), the Fundamental Research Funds for the Central Universities (No. 3132024218), and high-performance computing platform of Peking University.

Appendix A. Supplementary data

Supplementary data to this article can be found online at https://doi.org/10.1016/j.ijhydene.2025.05.206.

References

[1] Ge Y, Ma H, Wang L. Experimental and numerical investigation of combustion characteristics of carbon-free NH3/H2 blends in N2O. Int J Hydrogen Energy 2024;49(1):510–20.
[2] Shah ZA, Mehdi G, Congedo PM, Mazzeo D, De Giorgi MG. A review of recent studies and emerging trends in plasma-assisted combustion of ammonia as an effective hydrogen carrier. Int J Hydrogen Energy 2024;51(1):354–74.
[3] Mikulčić H, Baleta J, Wang X, Wang J, Qi F, Wang F. Numerical simulation of ammonia/methane/air combustion using reduced chemical kinetics models. Int J Hydrogen Energy 2021;46(45):23548–63.
[4] Li T, Duan Y, Wang Y, Zhou M, Duan L. Research progress of ammonia combustion toward low carbon energy. Fuel Process Technol 2023;248(1):107821.
[5] Zhang R, Chen L, Li J, Hu X, Wei H, Pan J. Optical study on the effects of wall and intake temperatures on ammonia combustion and emissions. Energy Fuel 2024;38(11):10333–44.
[6] Zuo W, Qiao Y, Yuan D, Hua J, Deng C, Lyu X. Effect of oxygen concentration on ammonia combustion: a combined ReaxFF and DFT study. Int J Hydrogen Energy 2024;79(1):1155–64.
[7] Osipova KN, Zhang X, Sarathy SM, Korobeinichev OP, Shmakov AG. Ammonia and ammonia/hydrogen blends oxidation in a jet-stirred reactor: experimental and numerical study. Fuel 2022;310(1):122202–15.
[8] Kang L, Pan W, Zhang J, Wang W, Tang C. A review on ammonia blends combustion for industrial applications. Fuel 2023;332(1):126150–75.
[9] Ariemma GB, Sorrentino G, Ragucci R, de Joannon M, Sabia P. Ammonia/Methane combustion: stability and NOx emissions. Combust Flame 2022;241(1):112071–84.
[10] Hayakawa A, Goto T, Mimoto R, Kudo T, Kobayashi H. NO formation/reduction mechanisms of ammonia/air premixed flames at various equivalence ratios and pressures. Mech Eng J 2015;2(1):14–402. 00414-00402.
[11] Wang G, Guiberti TF, Cardona S, Jimenez CA, Roberts WL. Effects of residence time on the NOx emissions of premixed ammonia-methane-air swirling flames at elevated pressure. Proc Combust Inst 2023;39(4):4277–88.
[12] Radwan AM, Paul MC. Plasma assisted NH3 combustion and NOx reduction technologies: principles, challenges and prospective. Int J Hydrogen Energy 2024;52(1):819–33.
[13] Kobayashi H, Hayakawa A, Somarathne KDKA, Okafor EC. Science and technology of ammonia combustion. Proc Combust Inst 2019;37(1):109–33.
[14] Wang S, Wang Z, Elbaz AM, Han X, He Y, Costa M, Konnov AA, Roberts WL. Experimental study and kinetic analysis of the laminar burning velocity of NH3/syngas/air, NH3/CO/air and NH3/H2/air premixed flames at elevated pressures. Combust Flame 2020;221(1):270–87.
[15] Miller JA, Bowman CT. Mechanism and modeling of nitrogen chemistry in combustion. Prog Energy Combust Sci 1989;15(67):287–338.
[16] Glarborg P, Miller JA, Ruscic B, Klippenstein SJ. Modeling nitrogen chemistry in combustion. Prog Energy Combust Sci 2018;67(1):31–68.
[17] Mei B, Zhang J, Shi X, Xi Z, Li Y. Enhancement of ammonia combustion with partial fuel cracking strategy: laminar flame propagation and kinetic modeling investigation of NH3/H2/N2/air mixtures up to 10 atm. Combust Flame 2021;231(1):111472–82.
[18] Chen Y, Su Y, Sui C, Chen W, Zhang B. Flame and emission characteristics of preheated ammonia combustion based on chemical reaction network. Fuel Process Technol 2023;242(1):107652–64.
[19] Okafor EC, Naito Y, Colson S, Ichikawa A, Kudo T, Hayakawa A, Kobayashi H. Experimental and numerical study of the laminar burning velocity of CH4–NH3–air premixed flames. Combust Flame 2018;187(1):185–98.
[20] Wang D, Ji C, Wang S, Wang Z, Yang J, Zhao Q. Numerical study on the premixed oxygen-enriched ammonia combustion. Energy Fuel 2020;34(12):16903–17.
[21] Elbaz AM, Wang S, Guiberti TF, Roberts WL. Review on the recent advances on ammonia combustion from the fundamentals to the applications. Fuel Commun 2022;10:100053.
[22] Liu X, Wang G, Wang F, Li P, Si J, Hanif F, Mi J. Classification and characteristics of ammonia combustion in well stirred reactor. Int J Hydrogen Energy 2023;55(1):1–13.
[23] Zhang M, Xu W, Wang R, Wei X, Wang J, Huang Z, Tan H. Wall heat loss effect on the emission characteristics of ammonia swirling flames in a model gas turbine combustor. Combust Flame 2023;256(1):112955.
[24] Hayakawa A, Arakawa Y, Mimoto R, Somarathne KDKA, Kudo T, Kobayashi H. Experimental investigation of stabilization and emission characteristics of

ammonia/air premixed flames in a swirl combustor. Int J Hydrogen Energy 2017;42(19):14010–8.
[25] Tang R, Xu Q, Pan J, Gao J, Wang Z, Wei H, Shu G. An experimental and modeling study of ammonia oxidation in a jet stirred reactor. Combust Flame 2022;240(1):112007–17.
[26] Okafor EC, Tsukamoto M, Hayakawa A, Somarathne KDKA, Kudo T, Tsujimura T, Kobayashi H. Influence of wall heat loss on the emission characteristics of premixed ammonia-air swirling flames interacting with the combustor wall. Proc Combust Inst 2021;38(4):5139–46.
[27] Okafor EC, Somarathne KDKA, Ratthanan R, Hayakawa A, Kudo T, Kurata O, Iki N, Tsujimura T, Furutani H, Kobayashi H. Control of NOx and other emissions in micro gas turbine combustors fuelled with mixtures of methane and ammonia. Combust Flame 2020;211(1):406–16.
[28] Khateeb AA, Guiberti TF, Wang G, Boyette WR, Younes M, Jamal A, Roberts WL. Stability limits and NO emissions of premixed swirl ammonia-air flames enriched with hydrogen or methane at elevated pressures. Int J Hydrogen Energy 2021;46(21):11969–81.
[29] Zhu X, Khateeb AA, Guiberti TF, Roberts WL. NO and OH* emission characteristics of very-lean to stoichiometric ammonia–hydrogen–air swirl flames. Proc Combust Inst 2021;38(4):5155–62.
[30] Somarathne KDKA, Hatakeyama S, Hayakawa A, Kobayashi H. Numerical study of a low emission gas turbine like combustor for turbulent ammonia/air premixed swirl flames with a secondary air injection at high pressure. Int J Hydrogen Energy 2017;42(44):27388–99.
[31] García-Ruiz P, Uruén M, Abián M, Alzueta MU. High pressure ammonia oxidation in a flow reactor. Fuel 2023;348(1):128302–11.
[32] Park Y-K, Kim B-S. Catalytic removal of nitrogen oxides (NO, NO2, N2O) from ammonia-fueled combustion exhaust: a review of applicable technologies. Chem Eng J 2023;461:141958.
[33] Zhu X, Du J, Yu Z, Cheng Y-B, Wang Y. NOx emission and control in ammonia combustion: state-of-the-art review and future perspectives. Energy Fuel 2023;38(1):43–60.
[34] Li Z, Zhang Y, Zhang H. Kinetics modeling of NOx emission of oxygen-enriched and rich-lean-staged ammonia combustion under gas turbine conditions. Fuel 2024;355(1):129509.
[35] Thomas DE, Wadkar C, Goertemiller CFW, Northrop WF. Structure and nitric oxide formation in laminar diffusion flames of ammonia–hydrogen and air. Fuel 2024;362:130764.
[36] Shu Z, Dai C, Li P, Mi J. Nitric oxide of MILD combustion of a methane jet flame in hot oxidizer coflow: its formations and emissions under H2O, CO2 and N2 dilutions. Fuel 2018;234:567–80.
[37] Yan Y, Yin Z, Yang R, Ou J, Xie T, Liu Z, Liu J. Characteristics of fuel-borne nitrogen pollutants in hydrogen–ammonia mixtures using argon–oxygen atmosphere under engine conditions. J Energy Resour Technol, Part A: Sustainable and Renewable Energy 2025;1(2):022305.
[38] Yang R, Yan Y, Ou J, Liu Z, Liu J. Application of argon circulation to investigate fuel nitrogen oxides emission characteristics of ammonia spark ignition engines, vol. 32. SAE Technical Paper Series; 2023. p. 107.
[39] Zhao Z, Zhang T, Li X, Zhang L, Zhang Z, Chen Y, Wu F, Luo C, Zheng C. NO formation mechanism of CH4/NH3 jet flames in hot co-flow under MILD-oxy condition: effects of co-flow CO2 and H2O. Fuel 2022;313:123030.
[40] Yang R, Liu J, Liu Z, Liu J. Numerical investigation into the characteristics of fuel-borne nitrogen pollutants in ammonia-diesel dual fuel engines through implementing atmospheric nitrogen unreactivity. Proceedings of the ASME 2024. October 20-23, 2024. San Antonio, Texas.
[41] Li J, Huang H, Kobayashi N, He Z, Nagai Y. Study on using hydrogen and ammonia as fuels: combustion characteristics and NOxformation. Int J Energy Res 2014;38(9):1214–23.
[42] Yan Y, Yang R, Liu Z, Liu J. Nitrogen oxides emission characteristics of zero-carbon ammonia-hydrogen fuels for internal combustion engines. SAE Technical Paper Series; 2023.
[43] Yang R, Yan Y, Liu Z, Liu J. Formation and evolution of thermal and fuel nitrogen oxides in the turbulent combustion field of ammonia internal combustion engines, vol. 1. SAE Technical Paper Series; 2023. p. 192.
[44] Yang R, Liu J, Liu Z, Liu J. Applying separate treatment of fuel- and air-borne nitrogen to enhance understanding of in-cylinder nitrogen-based pollutants formation and evolution in ammonia-diesel dual fuel engines. Sustain Energy Technol Assessments 2024;69:103910.
[45] Yang R, Liu Z, Liu J. The methodology of decoupling fuel and thermal nitrogen oxides in multi-dimensional computational fluid dynamics combustion simulation of ammonia-hydrogen spark ignition engines. Int J Hydrogen Energy 2024;55:300–18.
[46] Wu B, Wang Y, Wang D, Feng Y, Jin S. Generation mechanism and emission characteristics of N2O and NO in ammonia-diesel dual-fuel engine. Energy 2023;284:129291.
[47] Zhang X, Moosakutty SP, Rajan RP, Younes M, Sarathy SM. Combustion chemistry of ammonia/hydrogen mixtures: jet-stirred reactor measurements and comprehensive kinetic modeling. Combust Flame 2021;234(1):111653–67.
[48] Turns SR. An introduction to combustion. New York, USA: McGraw-Hill Companies; 1996.
[49] Kee RJ, Coltrin ME, Glarborg P, Zhu H. Chemically reacting flow: theory, modeling, and simulation. England: John Wiley & Sons; 2017.
[50] Lindemann FA, Arrhenius S, Langmuir IRD, Perrin J, Lewis, W CM. Discussion on "the radiation theory of chemical action". Trans Faraday Soc 1922;17(1):598–606.
[51] Gilbert RG, Luther K, Troe J. Theory of thermal unimolecular reactions in the fall-off range. II. Weak collision rate constants. Ber Bunsen Ges Phys Chem 1983;87(2):169–77.
[52] Smith GP, Golden DM, Frenklach M, Moriarty NW, Eiteneer B, Goldenberg M, Bowman CT, Hanson RK, Song S, Gardiner Jr WC, Lissianski VV, Qin Z. GRI-Mech 3.0. http://www.me.berkley.edu/gri_mech/.1999; 2004.

Glossary

Symbols

r_f: Forward reaction rate
r_r: Reverse reaction rate
k_f: Forward reaction rate constant
k_r: Reverse reaction rate constant
[X]: Mole concentration of component X
M: Third body
X_n: Coefficient of the third body component n
k_{fi}: Forward reaction constant involving three-body collisions
k_{ri}: Reverse reaction constant involving three-body collisions
X_m: Mole fraction for species m
T: Temperature (K)
T_{coflow}: Coflow temperature (K)
T_{wall}: Wall temperature (K)
T_{PSR}: Temperature of perfectly stirred reactor (K)
r: Radial coordinate (mm)

Greek letters

Φ: Equivalence ratio
ε: Turbulent dissipation

Abbreviations

MILD: Moderate or intense low-oxygen dilution
CFD: Computational fluid dynamics
PSR: Perfectly stirred reactor
EDC: Eddy dissipation concept model
DO: Discrete ordinate model
WSGG: Weighted sum of gray gases model
QUICK: Quadratic upwind interpolation for convection kinetics scheme
ROP: Rate of production
RE: Relative error